Bio-Design and Manufacturing (2022) 5:174–188
https://doi.org/10.1007/s42242-021-00148-1

RESEARCH ARTICLE

# Bioinspired soft actuators with highly ordered skeletal muscle structures

Yingjie Wang[1,3] · Chunbao Liu[1,3] · Luquan Ren[3] · Lei Ren[2,3]

Received: 16 March 2021 / Accepted: 9 June 2021 / Published online: 17 July 2021


## Abstract

Mammals such as humans develop skeletal muscles composed of muscle fibers and connective tissue, which have mechanical properties that enable power output with three-dimensional motion when activated. Artificial muscle-like actuators developed to date, such as the McKibben artificial muscle, often focus sole contractile elements and have rarely addressed the contribution of flexible connective tissue that forms an integral part of the structure and morphology of biological muscle. Herein, we present a class of pneumatic muscle-like actuators, termed highly mimetic skeletal muscle (HimiSK) actuator, that consist of parallelly arranged contractile units in a flexible matrix inspired by ultrasonic measurements on skeletal muscle. The contractile units act as a muscle fiber to produce active shortening force, and the flexible matrix functions as connective tissue to generate passive deformation. The application of positive pressure to the contractile units can produce a linear contraction and force. In this actuator, we assign different flexible materials as contractile units and a flexible matrix, thus forming five mold actuators. These actuators feature three-dimensional motion on activation and present both intrinsic force–velocity and force–length characteristics that closely resebmle those of a biological muscle. High output and tetanic force produced by harder contractile units improve the maximum output force by up to about 41.3% and the tetanic force by up to about 168%. Moreover, high displacement and velocity can be generated by a softer flexible matrix, with the improvement of maximum displacement up to about 33.3% and velocity up to about 73%. The results demonstrate that contractile units play a crucial role in force generation, while the flexible matrix has a significant impact on force transmission and deformation; the final force, velocity, displacement, and three-dimensional motion results from the interplay of contractile units, fluid and flexible matrix. Our approach introduces a model of the presented HimiSK actuators to better understand the mechanical behaviors, force generation, and transmission in bioinspired soft actuators, and highlights the importance of using flexible connective tissue to form a structure and configuration similar to that of skeletal muscle, which has potential usefulness in the design of effective artificial muscle.

✉ Chunbao Liu
liuchunbao@jlu.edu.cn

✉ Lei Ren
lei.ren@manchester.ac.uk

1 School of Mechanical and Aerospace Engineering, Jilin University, Changchun 130022, China

2 School of Mechanical, Aerospace and Civil Engineering, University of Manchester, Manchester M13 9PL, UK

3 Key Laboratory of Bionic Engineering, Ministry of Education, Jilin University, Changchun 130022, China

**Graphic abstract**

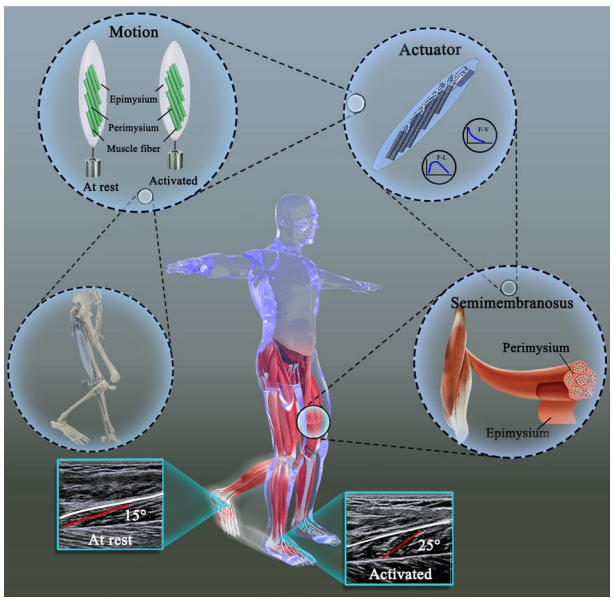


**Keywords** Bioinspired · Soft robotics · Actuator · Skeletal muscle

## Introduction

Skeletal muscles are highly versatile actuators. Humans can achieve slow or fast as well as flexible and powerful movements because their muscles possess mechanical properties capable of producing a broad range of mechanical output depending on three-dimensional motion, which is enabled by the complex interaction among muscle fibers, fluids, and flexible connective tissues [1–5]. Over the past two decades, many muscle-like actuators have been developed to mimic skeletal muscles to reproduce such mechanical properties. The McKibben artificial muscle developed in the 1950s was the first muscle-like actuator composed of sole contractile elements that could contract axially and expand radially in a similar manner to skeletal muscle when being pressured [6, 7]. This artificial muscle presented a force–length relation; however, the force–velocity relation differed from that of natural muscle [8]. Later varieties of the McKibben-based artificial muscle were proposed by changing its structure [9, 10], connecting artificial muscles together [11], and adding rigid elements, including DC motors, encoders and springs [12], or hydraulic dampers [8, 13]. These actuators only have a single contractile element, and it remains a challenge to realize both the force–velocity and force–length properties of skeletal muscle.

With the discovery of new materials and manufacturing technologies, further muscle-like actuators were developed to produce enhanced mechanical outputs, and many of these actuators can mimic the strain, force, and motion generated by skeletal muscle in one dimension. For example, a low-cost polymer fiber actuator that closely mimics skeletal muscle produced linear contraction and lifted 650 times its own weight, thus generating a strain of up to 1000% [14]. Peano-muscles [15, 16] are artificial muscles composed a simple plane mechanism that can produce linear contractions, show controllable linear contraction up to 10%, and lift 200 times their own weight. Pneumatic actuators work by negative or positive pressure. Negative pressure can make the volume of the fluidic chambers smaller or even reach zero; positive pressure can increase the fluidic chambers' volume until the maximum air pressure, or up to the ability of the materials to withstand the maximum pressure. Negative-pressure actuators are safer than positive-pressure actuators because they cannot rupture, since deformation stops when the fluidic chambers collapse to their minimum volume. Positive-pressure actuators are easily broken because they use high-pressure fluid. While negative-pressure actuators are limited by the negative pressure ($<0.1$ MPa), positive-pressure actuators use actuation pressures of up to 1 MPa. Therefore, the latter can achieve larger strokes, which are similar to those of natural muscle.

Both negative- and positive-pressure actuators are widely used because of their large actuation stresses and deformation [17, 18]. Vacuum-actuated muscle-inspired pneumatic structures utilize the buckling of elastomeric beams to generate linear motions [19], yet achieve a maximum actuation

stress of 65 kPa and contraction of 45%. Bubble artificial muscles [20] are designed to have a similar structure as pleated pneumatic artificial muscles, are lightweight, flexible, inexpensive, and are capable of contracting at a low pressure and generating a maximum contraction of 43.1% and a maximum stress of 0.894 MPa. These muscle-like actuators exhibit high strain and stress and produce linear contraction similar to that of real muscles. However, most studies focus on contractile elements and mistake these for the sole determinant of actuator contractile performance, whereas the flexible connective tissue that forms the complete structure and morphology [21] has not received sufficient attention or has often been overlooked. Few studies have aimed to construct actuators while focusing on their architecture, structure and morphology, or the forces occurring during muscular contraction. Therefore, there is a pressing need to design a highly mimetic muscle-like actuator that takes these aspects into consideration for the improved control of mechanical behaviors.

Herein, we introduce a highly mimetic skeletal muscle (HimiSK) actuator actuated by positive pressure. The actuator is inspired by ultrasonic measurement, which verifies that the skeletal muscle is flexible and composed of muscle fiber and connective tissue. Therefore, we designed a HimiSK actuator consisting of parallelly arranged series of contractile units with an ordered architecture in a flexible matrix. The contractile units act as muscle fibers to produce active contraction force when pressure is applied, and the flexible matrix acts as connective tissue, thus forming the complete structure and morphology of the actuator that produces passive deformation. HimiSK actuators use a material system for contractile units and a flexible matrix based on different silicone materials while sharing the same shapes as semimembranosus muscles, and are named as E, D, S, E-D, and D-S molds. These allow the analyses of the effects of interactions among the contractile units, flexible matrix and fluid on mechanical behaviors. These actuators present several features: i) Their mechanical properties (force–velocity and force–length relations) measured at different activation levels approach those of human skeletal muscles, show a structure, architecture, and configuration similar to skeletal muscle, and feature three-dimensional motion on activation. ii) By varying the materials of the contractile units, the output force and tetanic force can be boosted by increasing the hardness of contractile units. iii) By varying the material of the flexible matrix, the hardness of this matrix is decreased and the displacement and velocity can be subsequently increased. Our results demonstrate that the contractile units play a primary role in force generation, and the flexible matrix is important in the force transmission and interaction of contractile units, fluid, and flexible matrix that affect the actuator final force, velocity, displacement, and three-dimensional motion. This study proposes a new strategy to address the long-lasting challenge of achieving the optimal mechanical properties of actuators, and introduces a model to understand their mechanical behaviors, force generation, and transmission by varying their materials. The proposed actuators have a potential for a wide range of applications, including bioinspired robotics, active prostheses and exoskeletons, or rehabilitation robotics.

## Bioinspired design and operating principle

Skeletal muscle is considered as a soft actuator with flexible properties, that is, the Young's modulus of the semimembranosus, rectus femoris, and musculus gastrocnemius is about 10.12, 7.39, and 14.55 kPa as measured by ultrasound (Fig. 1a). Skeletal muscle is composed of muscle fibers and connective tissue in a composite hierarchical structure. Muscle fibers are arranged in parallel in flexible connective tissue at an angle relative to the muscle's line of action, called the pennation angle [22, 23]. Connective tissue, composed of perimysium and epimysium tissues [24, 25], surrounds the muscle fibers and the entire muscle to ensure that the muscle volume remains constant (Fig. 1a). The interaction between muscle fibers and flexible connective tissue shapes the three-dimensional motion of the muscle (Fig. 1b). When activated, muscle fibers decrease in length and increase in radius, and these changes must be accommodated by increases in one or more orthogonal directions. As shown in Fig. 1c, if a muscle increases in thickness (t: the distance between aponeuroses), the pennation angle rises as the muscle fibers shorten, resulting in the shortening of the muscle due to its constant volume. If the width (w) of a muscle increases, the pennation angle does not enlarge with fiber shortening, hence muscle shortening is less possible. The spatial arrangement of muscle fibers essentially determines the mechanical properties of the muscle [4, 11, 22, 26]. When the muscle changes in thickness, this contraction leads to an increase in the pennation angle, which is favorable to the velocity output as fiber rotation amplifies the velocity, but is less favorable to the force output because the increased pennation angle reduces the component of fiber force oriented along the vertical force line. When a muscle changes in width, the velocity output is relatively low due to the lack of amplification of velocity produced by fiber rotation; however, this situation is favorable to the force output because there is no reduction in the component of fiber force oriented along the vertical force line. This motion serves as an automatic transmission system, in which low loads are favorable to the velocity output and high loads are favorable to the force output.

Therefore, inspired by skeletal muscle, we designed a HimiSK actuator composed of a series of contractile units and a flexible matrix. In this design, the McKibben-based contractile units act as muscle fibers to generate

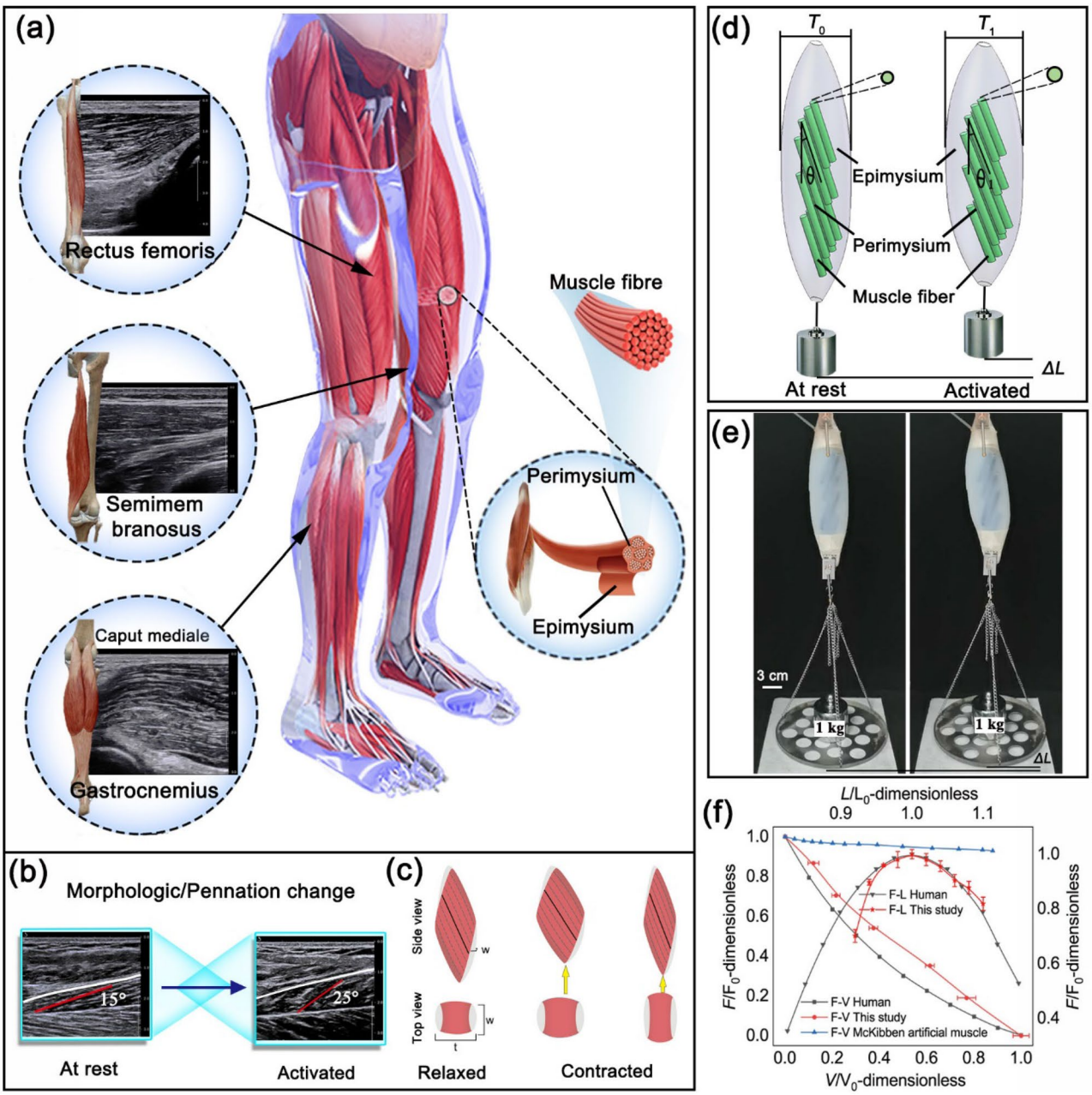


**Fig. 1** Design principle of a HimiSK actuator. **a** Ultrasound measurements of gastrocnemius, rectus femoris, and semimembranosus muscles. **b** Ultrasound image of human medial semimembranosus muscle measured in the sagittal plane. **c** A simplified model of a pennate muscle illustrating the orientation of fibers when relaxed and contracted, and explaining the action mechanism (adapted from [22], Copyright 2008, National Academy of Sciences). **d** Structural component diagram and motion principle of soft actuator. **e** Linear contraction and mechanical output of muscle-like actuator when pressured. **f** Mechanical properties of the actuator

contraction force; the flexible matrix, which surrounds the contractile units (representing the perimysium) and the entire actuator (representing the epimysium), acts as flexible connective tissue ensuring that the muscle volume remains constant. The contractile units and flexible matrix are connected by their materials self-integrated. Different flexible materials are chosen for actuators leading to deformation and changes in mechanical behaviors, including force and velocity, stress, and strain. The HimiSK actuator operates under air pressure, as shown in Fig. 1d. When air pressure is applied at low loads, the McKibben-based contractile units shorten in length and expand in diameter, similarly to muscle fibers. Therefore, the flexible matrix increases in thickness ($T_0$ to $T_1$), and the contractile unit rotates as the pennation angle increases ($\theta$ to $\theta_1$), leading to the actuator shortening

in length ($\Delta L$) because of the constant volume of the flexible matrix. The forces generated by contractile units are transmitted by the flexible matrix to produce a mechanical output as shown in Fig. 1e. The semimembranosus HimiSK actuator (D mold) can lift a 1.0 kg weight at 0.28 MPa, and presents both force–length and force–velocity properties that are comparable to those of human muscle but are absent from the McKibben artificial muscle (Fig. 1f). This indicates that actuator is successfully achieved mechanical output and mechanical properties.

## Materials and fabrication

The fabrication of the proposed HimiSK actuator follows a basic principle (Fig. 2a). The manufacturing method can be used to shape actuators with arbitrary muscle architectures, structures, (unipennate, bipennate, and multipennate muscles), and configurations using different flexible materials. To construct the actuator with a given design, the HimiSK actuator was fabricated by casting [27] (Fig. 2b). The actuator mainly consists of contractile units and a flexible matrix. The contractile unit can be cast from a variety of materials (Fig. 2b, casting; Table 1). It can be assembled with an elastic hose (inner diameter: 4 mm, outer diameter:

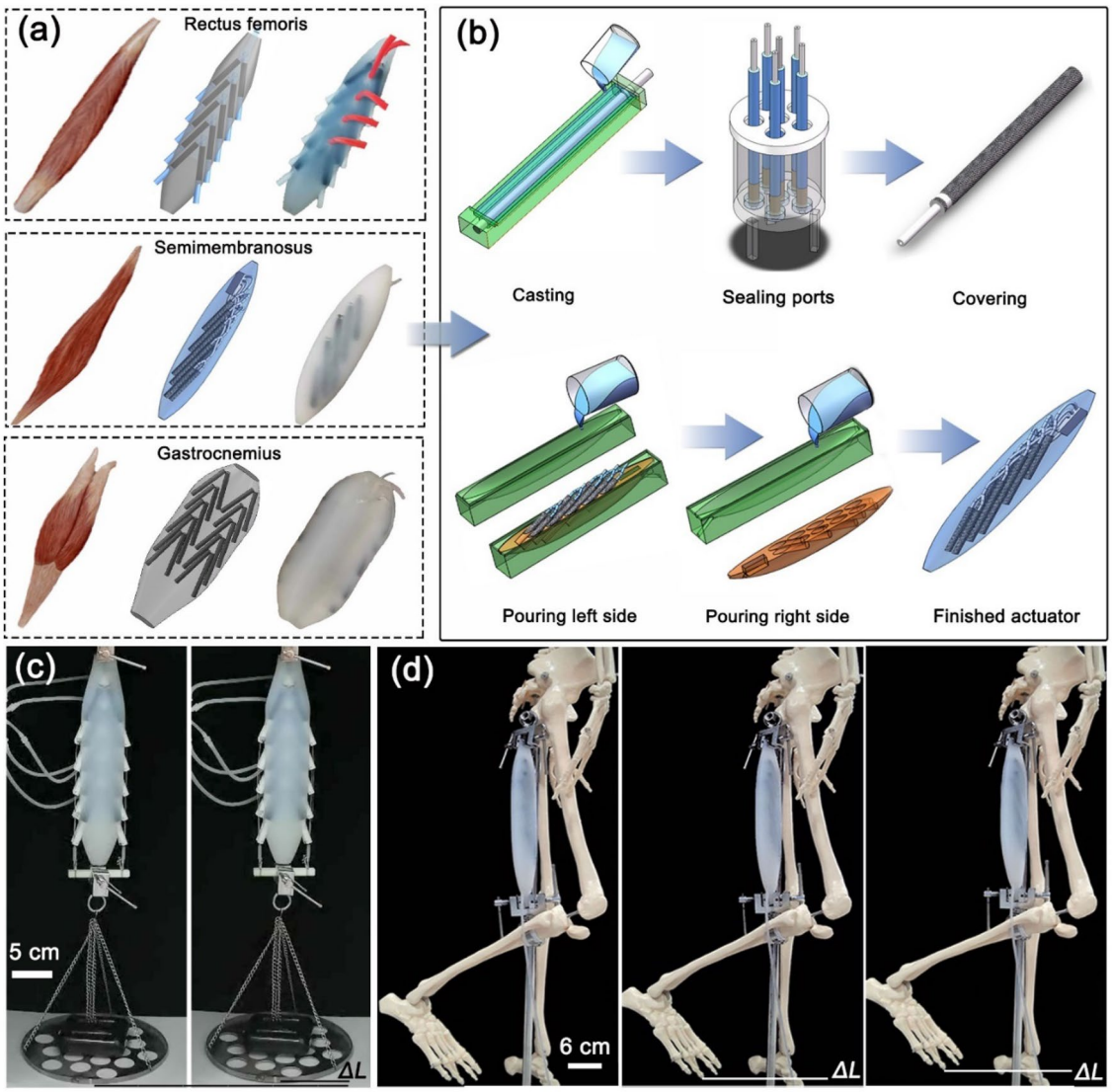


**Fig. 2** Fabrication and motion of a muscle-like actuator. **a** The actuators of gastrocnemius, rectus femoris, and semimembranosus muscle. **b** Fabrication of semimembranosus actuator. **c** The rectus femoris actuator lifting weights. **d** The semimembranosus actuator acting in a physical anatomical human model to flex the knee joint; $\Delta L$ represents actuation strain

**Table 1** Properties of three types of silicone rubber (as declared by the manufacturer)

| Type | Volume mixing ratio | Curing time | Mixed viscosity | Pot life | Shore hardness | Elongation at break | Tensile strength |
|---|---|---|---|---|---|---|---|
| Ecoflex00-30 | 1A:1B | 4 h | 3000 cps | 45 min | 0–30 | 900% | 200 psi |
| Dragonskin20 | 1A:1B | 4 h | 20,000 cps | 25 min | 20 A | 620% | 550 psi |
| Smmothsil40 | 100A:10B | 24 h | 35,000 cps | 30 min | 40 A | 300% | 600 psi |

6 mm, length: 90 mm) and a woven mesh (angle: 45°). The elastic hose, whose ends are sealed by the same material (Fig. 2b, sealing ports), is coated in a woven mesh. The woven mesh can be closed with a ribbon (Fig. 2b, covering) to limit the inflation of the elastic hose that shortens in length and expands in diameter, allowing the production of linear contraction when air pressure is applied. The length of each fabricated contractile unit was approximately 90, 70, and 50 mm. Five sets of contractile units were placed sequentially in the order of 50, 70, 90, 70, and 50 mm with a pinnation angle of 20° in a double row. Each set consisting of two identical contractile units was connected by a three-way joint (Y-metric 1.5). There are five air inlets for five sets of contractile units. A six-way joint (SL1.6) connects to the five sets of contractile units to form one complete air inlet. When the actuation pressure is applied through the air only inlet, the five sets of contractile unit contract together. Finally, these contractile units can be connected together and fixed by the flexible matrix, which can also be constructed from different materials (Table 1) and should have sufficient flexibility in comparison with that of the contractile units.

The molds for fabricating the flexible matrix were composed of three parts (left and right molding parts and one core part). First, the left molding part was cast with a degassed elastic material (Table 1; Fig. 2b, pouring left side). Once cured, the two molds were separated, the core part was removed, and the right molding part was filled with elastic material (Fig. 2b, pouring right side); the left and right molds were then combined and cured at room temperature. The finished muscle-like actuator consisted of ten contractile units embedded in a flexible matrix with a length of 225.28 mm, maximum width of 60 mm, and volume of 221,300 $mm^3$ (Fig. 2b, finished actuator). Mimics of both the rectus femoris and semimembranosus muscles were shown to achieve a linear contraction similar to that of skeletal muscle when air pressure was applied (Figs. 2c and 2d). We combined three types of contractile units with three types of flexible matrix to produce five different muscle-like actuators (Table 2). The actuator enclosed reinforcement tapes at both ends to ensure that the actuator maintained the original shape of both sides after actuation. Using this fabrication method, a wide variety of actuators can be constructed.

## Experimental tests on HimiSK actuators

The force, displacement, and force–velocity properties for five actuators were tested using a customized experimental test-rig (Figs. 3a, 3b, and 3e). The displacement of the semimembranosus HimiSK actuator was measured via a laser displacement sensor (HG-C1100, Panasonic, Japan) and data were collected using a VIBSYS vibration signal acquisition instrument (Beijing Bopu Ltd., China). The force was measured by a pressure sensor (CG Q-YS, Bengbu Tongli Ltd., China), which was connected to the DYB-5 dynamic strain gage (Beidaihe Electronics Ltd., Hebei, China). The five different actuators have different capabilities for bearing maximum pressure and load. The maximum pressure of the E mold was approximately 0.1 MPa, which corresponded to a maximum load of 1.8 kg. The maximum pressure of the D and E-D molds was 0.28 MPa, which corresponded to maximum loads of 4.4 and 2.2 kg loads, respectively, while the maximum pressure of the S and D-S molds was 0.48 MPa with a maximum load of 6.2 and 6.5 kg, respectively. The maximum pressure was divided into five levels. The maximum load that could be lifted by the actuator under each pressure level was equally divided into six different loads. Each contraction was repeated six times.

A separate customized experimental test-rig was constructed to measure the force–length performance of fabricated actuators (Figs. 3c–3e). The force–length relationship describes the relationship between the maximum isometric force that can be obtained for a given muscle length. The actuator was fixed at both ends to maintain a constant length

**Table 2** Five types of soft actuator consisting of different materials

| Actuator | E mold | E-D mold | D mold | D-S mold | S mold |
|---|---|---|---|---|---|
| Contractile unit | Ecoflex00-30 | Dragonskin20 | Dragonskin20 | Smoothsil40 | Smoothsil40 |
| Matrix | Ecoflex00-30 | Ecoflex00-30 | Dragonskin20 | Dragonskin20 | Smoothsil40 |

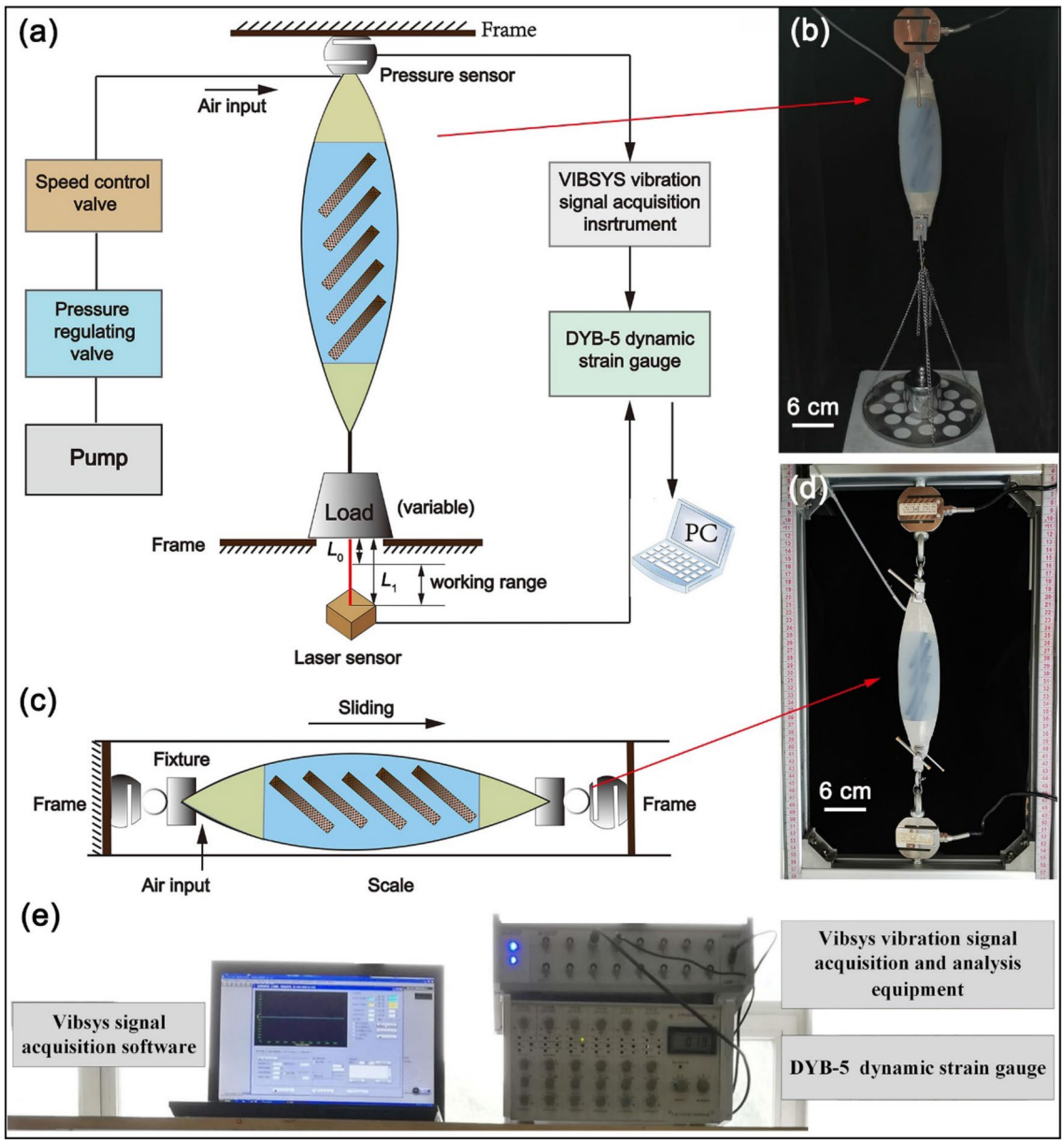


**Fig. 3** Schematic diagram of the experimental system. (**a, b**) Measurement of the force–velocity relationship during isotonic contraction. (**c, d**) Measurement of the force–length relationship during isometric contraction. (**e**) Experimental equipment

and was contracted in a horizontal direction. In the initial state, the soft actuators were kept level with the length of each increased by three millimeters, and were each tested at ten different lengths; the actuator length was adjusted by repositioning the two movable ends. The output force was measured at each constant length. The initial length was defined as the actuator length minus the length of the taps (45 mm). The pressure measured in the force–length experiment was lower than that in the force–velocity experiment because of the large tensile force. The E mold soft actuator was tested at pressures of 0.02, 0.04, and 0.06 MPa; the pressures of D and E-D mold were tested at 0.12, 0.16, and 0.20 MPa; and the maximum pressures of S and D-S mold were tested at 0.24, 0.32, and 0.40 MPa.

The results were uploaded to a PC (Fig. 3a), and the output force and the displacement obtained during each contraction was analyzed using MATLAB software (MathWorks, Inc., USA). The actuator shortening velocity was calculated as the actuator contraction displacement between the two frames divided by the isotonic contraction time. The actuator force and shortening velocity for the E, D, and S mold actuators are presented in Fig. 4. A peak shortening velocity zone with a duration of 0.1 s was defined where the maximum shortening velocity was achieved in the middle of the zone,

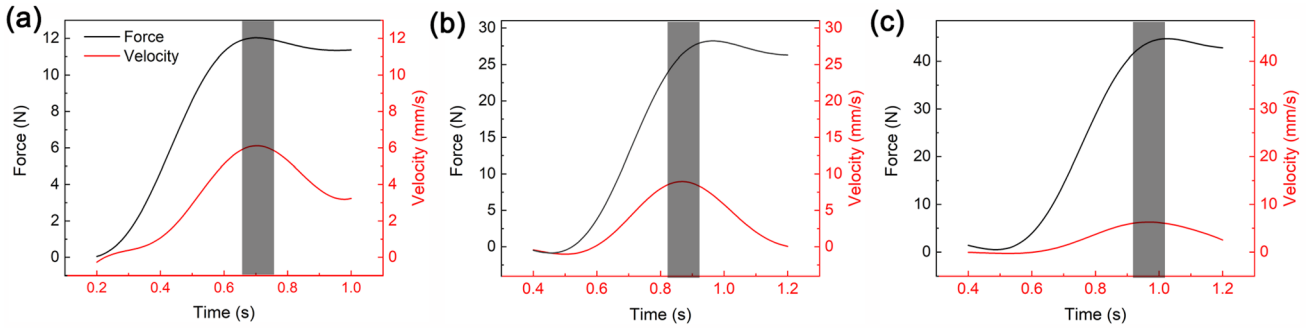


**Fig. 4** Representative force and velocity analysis. **a** E mold under 1.2 kg at 0.1 MPa. **b** D mold under 2.6 kg at 0.28 MPa. **c** S mold under 4.5 kg at 0.48 MPa

while the actuator force reached a steady state. Thereafter, the average shortening velocity and average force within this zone were used to quantify the actuator force–velocity characteristics.

The three-dimensional motions of D mold actuator over time under zero load at 0.28 MPa are shown in Fig. 5a. With gas pressure applied, the actuators show three-dimensional deformation in space rather than simply vertical linear contraction. The dimensionless relationship between the maximum force and contraction velocity of the D, S, E, E-D, and D-S type actuators compared with that of human skeletal muscle models is illustrated in Fig. 5b [28]. The maximum force ($F_0$) was adopted from the force–length test at the same actuation pressure. The results for these actuators indicate a similar shape with skeletal muscles, which is missing in the McKibben artificial muscle. This behavior highlights the ability of the HimiSK actuator to automatically vary the force and the velocity in response to variable loads. The dimensionless relation between the maximum force and length of the E, D, S, E-D, and D-S mold actuators during isometric contraction, compared with that of human skeletal muscle models and the McKibben pneumatic artificial muscle, is illustrated in Fig. 5c [28]. The bio-muscle-like actuator has a parabolic-shape force–length relation that is very close to that of human muscle. The force–velocity and force–length relation obtained by changing the materials are also very similar to those of biological muscle, highlighting the excellent behavior of these actuators that is attributed to their architecture [22], structure [24], and configuration comparable to those of skeletal muscle [29].

## Simulation analysis of deformation

We built a finite element method (FEM) using ABAQUS software to investigate the deformation response of the HimiSK actuator to external loads. To simulate the response of the actuator to increased air pressure, we modeled the contractile unit as closed circular tubes driven by a fluid cavity, which is capable of simulating pressured gas or liquid behavior. Double symmetrical layer rebars were used to model the woven meshes wrapped around the contractile units, which had a Young's modulus of 100 MPa and Poisson's ratio of 0.3. The flexible matrix of E, D, and S mold actuators was defined as linear elastic material (Young's modulus of 0.25, 0.85, and 1.1 MPa, respectively; Poisson's ratio of 0.475). The interaction between the contractile units and the flexible matrix was defined as a tie constraint. The contractile units and the flexible matrix were meshed using a total number of 1136 and 31,407 tetrahedral quadratic (C3D10) elements, respectively. In all experiments, the top end of the actuator was fixed, while the load was applied at the bottom end. The deformations of the D mold actuator under six external loads applied in the tests are shown in Fig. 6a. All of the actuators presented the three-dimensional motion, and the deformation decreased with the increasing load. To further predict the deformation of these actuators, we built a model-based simulation (Figs. 6b and 6c) of the deformation of five actuators at their maximum applied pressures. The comparisons of the deformations of the D mold actuator between the test (Fig. 6a) and the simulation (Fig. 6b) showed that they all undergo similar deformation under each load. All of the model-based simulations reveal similar deformations, all decreasing with the load increasing (Figs. 6b and 6c), which is in good agreement with the experimental results. The notably large tensile deformation present in the E-D mold (blue area at 0.28 MPa) is caused by the softness of the material making it unable to resist large external loads. The load-dependent changes in the vertical displacement can be used to predict deformation. As expected, the degree of displacement decreases as the load increases (Fig. 6d). We also compared the experimental and simulated displacements for each actuator (Fig. 6e). As shown in most of the comparisons, the FEM simulations accurately predicted the displacement with negligible error and were consistently matching with the experimental data at different loads.

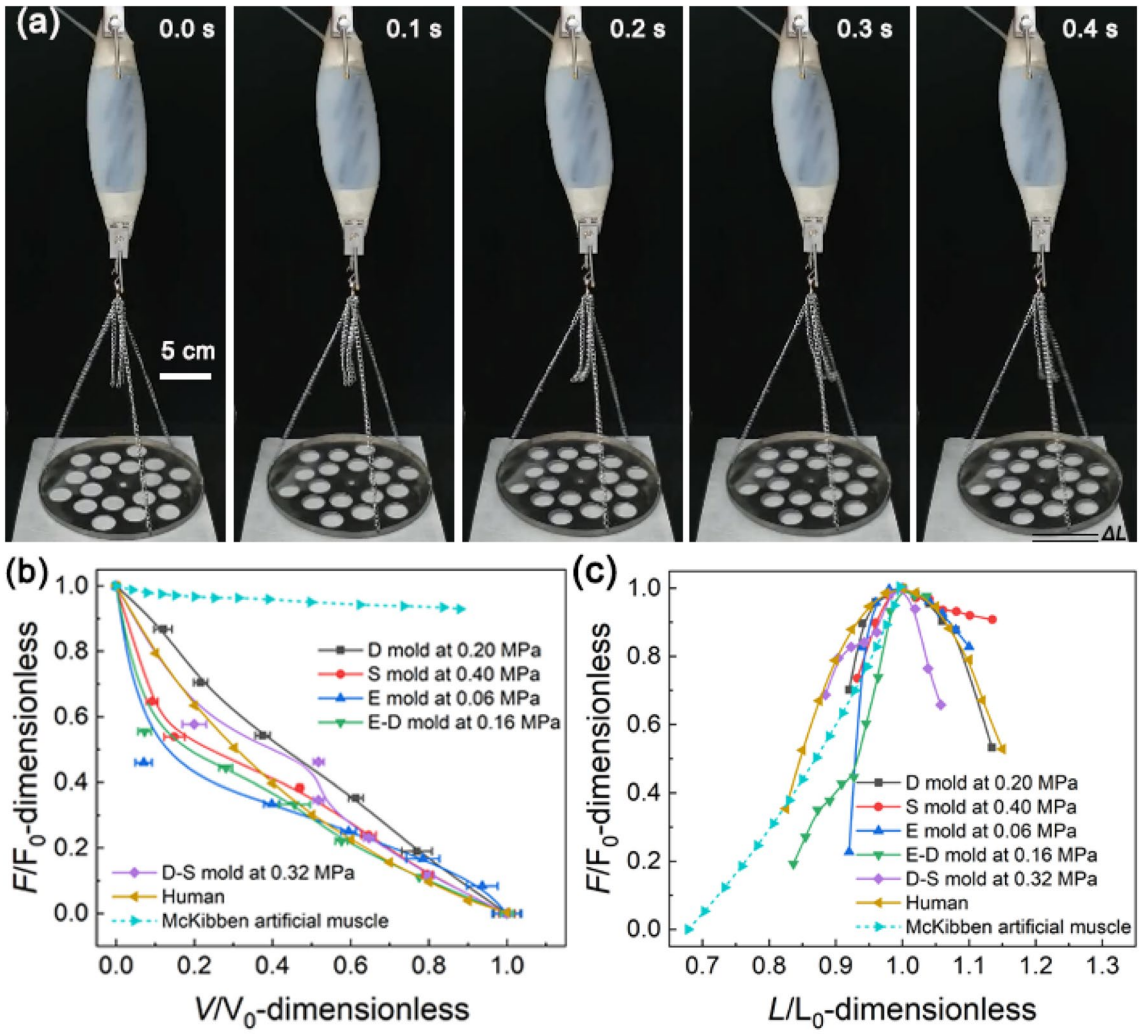


**Fig. 5** **a** Three-dimensional motion of the D mold actuator over time under zero load at 0.28 MPa; $\Delta L$ represents actuation strain. **b** The dimensionless relation between the maximum force and contraction velocity of muscle-like actuators compared with that of a human muscle. **c** The dimensionless relation between the maximum force and contraction length of five types muscle-like actuator compared with that of a human muscle

Simulations for the five actuators under different loads demonstrated that the interaction of the flexible matrix and contractile units play an important role in the deformation performance. The contractile units shorten in length and expand in diameter during rotation, resulting in the deformation of the actuator when air pressure is applied. Notably, contractile units with harder materials produced a greater force, while softer flexible matrix materials produced a greater displacement. For example, the D-S mold lifting 13 N loads presented more than 6 mm of displacement, whereas the D mold force only produced approximately 3 mm of displacement under about 13 N loads at their highest pressures. Meanwhile, soft and more flexible matrix materials produced a greater displacement. The E-D mold produced a displacement of more than 10 mm (0 N), whereas the D mold generated less than 6 mm of displacement at the same pressure.

## Characteristics of HimiSK actuators

### Strain and output force

We quantified the maximum strain for contractile units using vernier calipers as shown in Fig. 7a. As expected, the strain values of the E, D, and S contractile units were approximately the same (23%, 21%, and 20%, respectively), and ensured a consistency of deformation of the contractile units at 0.1, 0.28, and 0.48 MPa, respectively (Fig. 7b). Figure 7c presents the contraction of the soft actuators, where

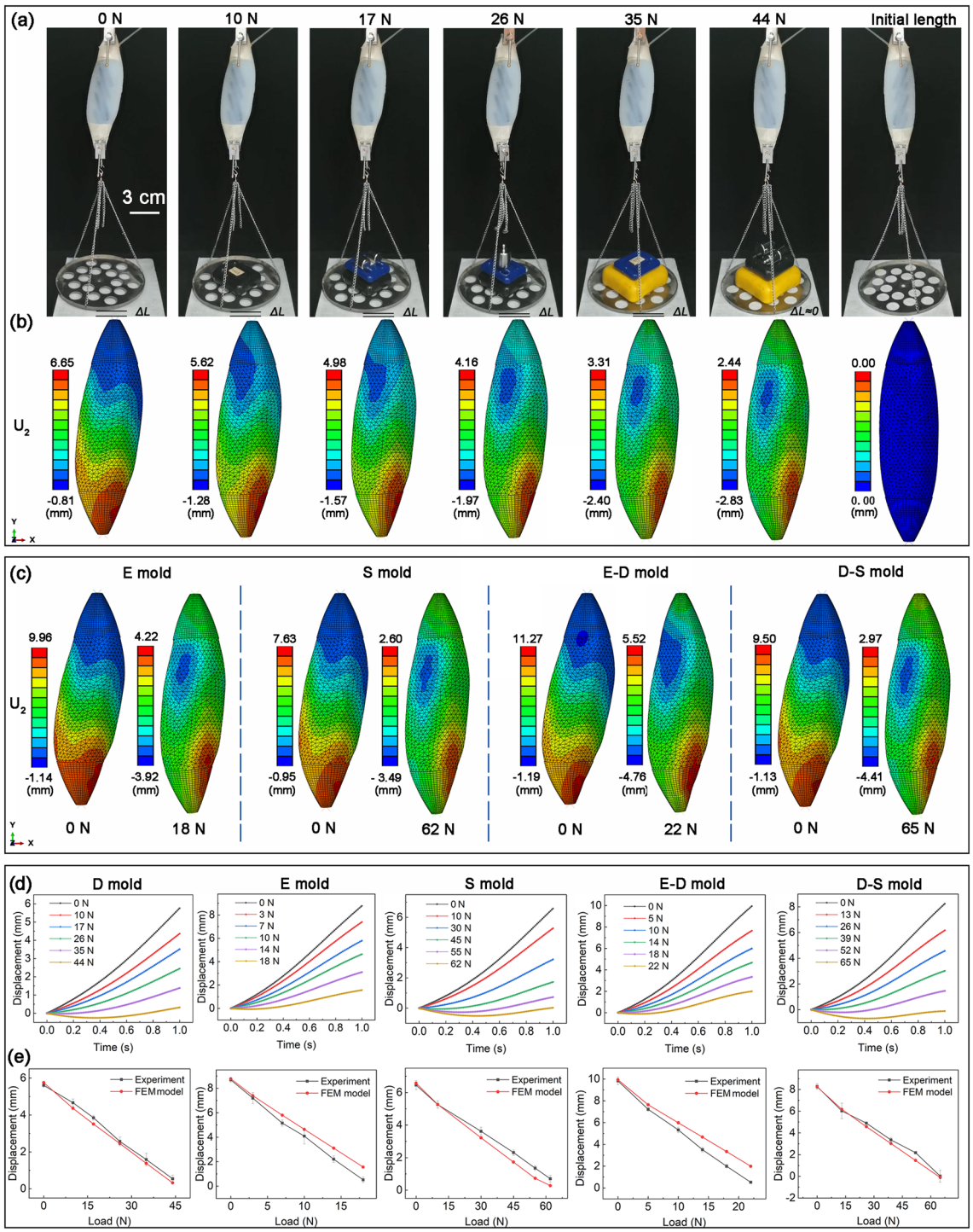


**Fig. 6** Actuator simulations. **a** D mold actuator deformation experiment at the highest pressure; $\Delta L$ represents actuation strain. **b** D mold actuator deformation using FEM modeling at the highest pressure. **c** E, S, E-D, and D-S mold actuator deformation using FEM modeling at the highest load and 0 load at the highest pressure. **d** Displacement of five types of actuators at different loads using FEM modeling at the highest pressure. **e** Comparison of actuator displacements between experimental measurements and FEM model predictions

the strain values measured for the E, D, and S mold actuators were approximately 4.6%, 3.0%, and 3.4% (Fig. 7d) and the output forces were approximately 1.8, 4.6, and 6.2 kg (Fig. 7e). These results demonstrate that each actuator has specific advantages on different scales, yielding an optimal performance of producing high strain and output force. The

E, D, and S molds performed optimally at 0–0.1, 0.1–0.28, and 0.28–0.48 MPa, respectively (Figs. 7d and 7e). Thus, the choice of actuator depends on the strain and force requirements.

In order to further investigate the influence of the flexible matrix, we compared actuators from the E-D and D-S molds with those from the E, D, and S molds. The E-D mold, which has the same contractile units as the D mold, experienced a strain of 5.20%, which is a 42.3% improvement over that of the D mold at 0.28 MPa (Fig. 7f). The E-D mold, which has the same flexible matrix as the E mold, exerted a force of 22 N, which is an about 22.2% improvement over that of the E mold under maximum pressure. However, its output force was lower than that of the D mold (Fig. 7g) due to the large tensile deformation (Fig. 6c, E-D mold), which contributed to the loss of output force. In a similar fashion, the D-S mold had a maximum strain of 5.1%, which consists a 33% improvement over that of the S mold at 0.48 MPa (Fig. 7h). Moreover, when lifting a 65 N load, it exhibited a 41.3% improvement in force compared with that of the D mold. Figure 7i presents the output force produced by the D-S mold and S mold when the output force is approached. As clearly seen, the harder materials of the contraction units contribute to force generation, while the softer materials of the flexible matrix support the force transmission and deformation. These results verify the presence of actuation and transmission mechanism in the HimiSK actuators as in skeletal muscle. The softer materials of the flexible matrix can favor the force transmission and contractile unit rotation, thus producing large deformation. This supports the idea that the mechanical output generated by skeletal muscle depends not only on force generation [30] but also on force transmission [31–33]. Accordingly, the D-S mold actuator has excellent performance in producing high strain and stress (Table 3).

Excluding strain and stress, the maximum power density, work density, and strain rate of HimiSK actuators were measured and compared with those of skeletal muscle and pneumatic artificial muscle (PAM). Due to the addition of flexible matrix, a gap was observed as compared to the PAM. This addition introduced limitations such as increased weight and volume, reduced strain, and large deformation produced where loads are applied. Nevertheless, the addition of a flexible matrix enables the favorable mechanical properties of the actuator to be realized, which are similar to those of skeletal muscle. Future work is planned to address these limitations by increasing the number of muscle contractile units to reduce the relative occupied volume of the flexible matrix, and to improve the force-generating capability using the D-S materials system. The development of techniques to mimic skeletal muscle tendons can eliminate the problem of large deformations where loads are applied, and achieve the direct transmission of force.

## Force–velocity and force–length

In order to characterize the velocity and force–velocity relationships of different material actuators, we conducted a test on five types of actuators using various loads at different air pressures (Figs. 8a–8e). Findings show that the force exhibits a consistent decreasing pattern with increasing velocity across different levels of activation pressures. As in skeletal muscle, the force and velocity produced by actuators are roughly inversely proportional. The output force rises with increasing activation level, and the maximum force ($F_0$) is generated at very low speed during forceful contractions, whereas zero force is produced at maximum contraction velocity ($V_0$). This force–length characteristic is one of the main advantages of this type of soft actuator, just like skeletal muscles. These results also indicate that the exceptional mechanical properties of the produced force–velocity can be attributed to our bioinspired design combining the contractile units with a flexible matrix. The comparison of velocities across different actuators that share the same contractile units (D is contractile unit actuator and S is contractile unit actuator) but have a different flexible matrix are shown in Fig. 8f. The velocity of the E-D mold actuator consists an about 87% improvement over that of the D mold actuator at 0.28 MPa, whereas the velocity of D-S mold actuator shows an about 73% improvement over that of the S mold actuator at 0.48 MPa. These results reveal that a softer flexible matrix is favorable for contractile unit rotation and thus facilitates the changes of pennation angle, which in turn amplifies the velocity of the soft actuator.

The force–length relationship and tetanic force of the five types of muscle-like actuator at different actuation pressures are shown in Figs. 9a–9e. These results indicate a consistent parabolic form across different levels of activation pressures, which is similar to that seen in skeletal muscle; the output force is larger at higher activation levels. The muscle length at the maximum tension is defined as the resting length ($L_0$), and the force decreases when the muscle length ($L$) is greater than the resting length. The maximum force is the highest value that corresponding to an optimal fiber. This can be stretched beyond the resting length, although great differences were observed between the results of various types. High-quality intrinsic biological properties can be obtained by varying the contractile units and flexible matrix materials; our results verify that the generation of optimal force–length properties is associated with the bioinspired design that has a similar shape, architecture and structure as skeletal muscle. The comparison of force between actuators with the same flexible matrix (E flexible matrix actuator and D flexible matrix actuator) but different contractile units is presented in Fig. 9f. The tetanic force of the E-D mold actuator shows an about 30% improvement over that of the E mold actuator at the highest pressure, and the tetanic force of the D-S mold

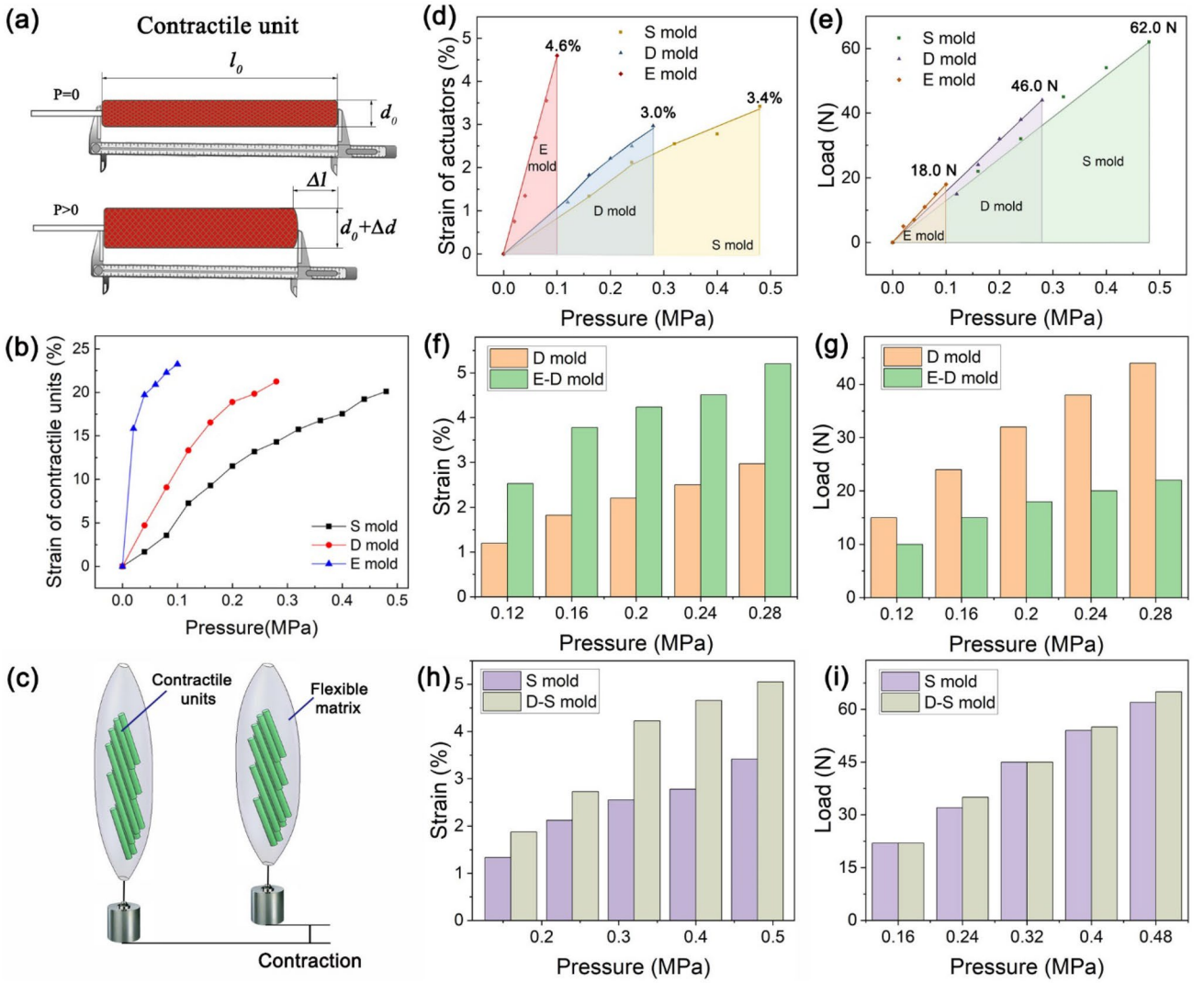


**Fig. 7** Output force and strain performance of muscle-like actuators. (**a**) Measurement of a contractile unit. (**b**) Relationship between contraction rate and pressure of contractile units. (**c**) Contraction of actuator. (**d**) Relationship between the strain and actuation pressure of E, D, and S actuators. (**e**) Relationship between the load and pressure of E, D, and S mold actuators. (**f, g**) Comparison of strain and output force over pressure between D and E-D mold actuator. (**h, i**) Comparison of strain and output force over pressure between S and D-S mold actuator

actuator constitutes an about 168% improvement over that of the D mold actuator at the highest pressure. The results demonstrate that the contractile unit with increased hardness enhances the capacity of force generation.

## Discussion

In this paper, we introduced a new class of actuators inspired by skeletal muscle. In contrast to previous pneumatic artificial muscles with sole contractile elements, the HimiSK actuator consists of a series of contractile units and a flexible matrix. We presented five types of actuators prepared from different materials but having the same shape based on a semimembranosus muscle (E, D, S, E-D, and D-S molds). In comparison with current artificial muscle designs, the semimembranosus HimiSK actuator exhibits several promising qualities. (i) Actuators can perform a three-dimensional motion that depends on their structure, architecture, and configuration resembling those of skeletal muscle, and with intrinsic mechanical properties that approximate those of biological muscle, thus making them unique in the field of muscle-like actuators. (ii) By the application of different contractile unit materials, the pressure bearing capability of these actuators is harnessed to increase their capability of force generation. For example, at the extreme pressure, the E-D mold actuator increased the output force and tetanic force by

**Table 3** The parameters of skeletal muscles and results for three types of soft actuator

| | Type | Mass (kg) | Stress (MPa) * | Strain (%) | Power density (W kg $^{-1}$) # | Work density (kJ m$^{-3}$) & | Strain rate (% s $^{-1}$) + |
|---|---|---|---|---|---|---|---|
| Skeletal muscle | Typical | – | 0.1 | 20 | 50 | 8 | Max. > 50 |
| PAM | – | – | 3.4 | 15 | 10e$^3$ | 500 | – |
| Soft actuators | E mold | 0.20 | 0.018 | 4.6 | 0.47 | 2.93 | 10 |
| | E-D mold | 0.20 | 0.022 | 5.2 | 0.83 | 9.87 | 5 |
| | D mold | 0.21 | 0.044 | 3.0 | 1.17 | 7.76 | 4 |
| | D-S mold | 0.21 | 0.066 | 5.1 | 2.76 | 19.70 | 16 |
| | S mold | 0.23 | 0.063 | 3.4 | 1.38 | 17.37 | 10 |

*The stress of a soft actuator is written as $\sigma = F/S$ (where $F$ represents the output force, and $S$ represents the maximum cross sectional area). #The power density of soft actuator is expressed as $P = Fv/m$ (where $F$ represents the output force, $v$ represents the velocity, and $m$ represents mass of actuator). &The work density is written as $W_{(in)} = \sum_{i=1}^{10} \int p\Delta v \mathrm{d}v/V_a$ (where $p$ represents the relative pressure, $v$ represents the volume change, and $i$ represents the number of contractile units, $V_a$ represents the volume of actuator), the $p$ and $V$ are collected from simulation. +The strain rate is formulated as $\varepsilon(t) = v(t)/L_1$ (where $v(t)$ represents the velocity, and $L_1$ represents the initial length of soft actuator)

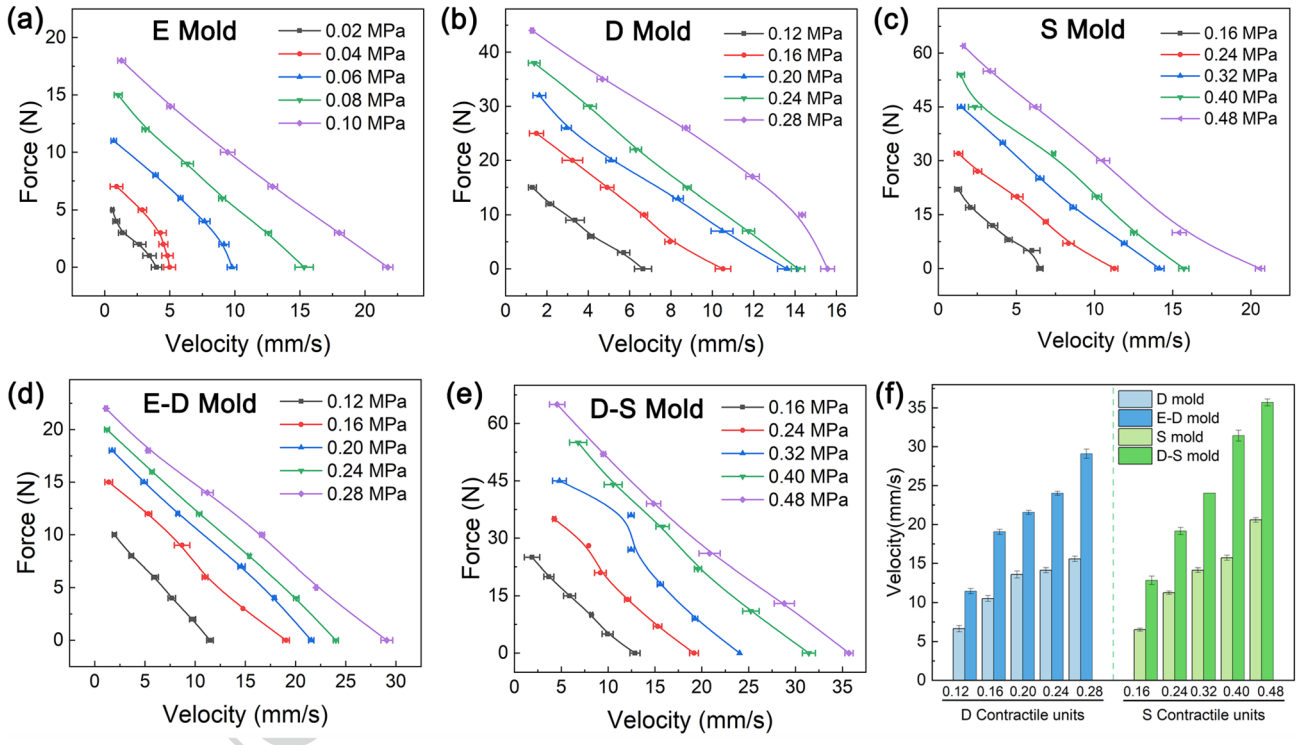


**Fig. 8** Relationship between the force and velocity of five muscle-like actuators. (**a–e**) Force–velocity properties of E, D, S, E-D, and D-S molds under different actuation pressures. (**f**) Comparison of velocity over the flexible materials of D contractile unit actuator and S contractile unit actuator

up to about 22.2% and about 30%, respectively, compared with that of the E mold. Moreover, the D-S mold actuators increased their output force and tetanic force by up to about 41.3% and about 168%, respectively, compared with D mold actuators. High force can therefore be produced by using harder contractile units. (iii) The capability of actuators for deformation can be exploited by the application of different flexible matrix materials. For instance, the E-D mold actuators increased the strain by up to about 42.3%, and their velocity was improved by about 87% of that of the D mold. Meanwhile, the D-S mold actuators can increase their strain by up to about 33.3%, which improves their velocity by up to about 73% compared with that of the S mold. High displacement and velocity can therefore be produced with a softer flexible matrix, which principle

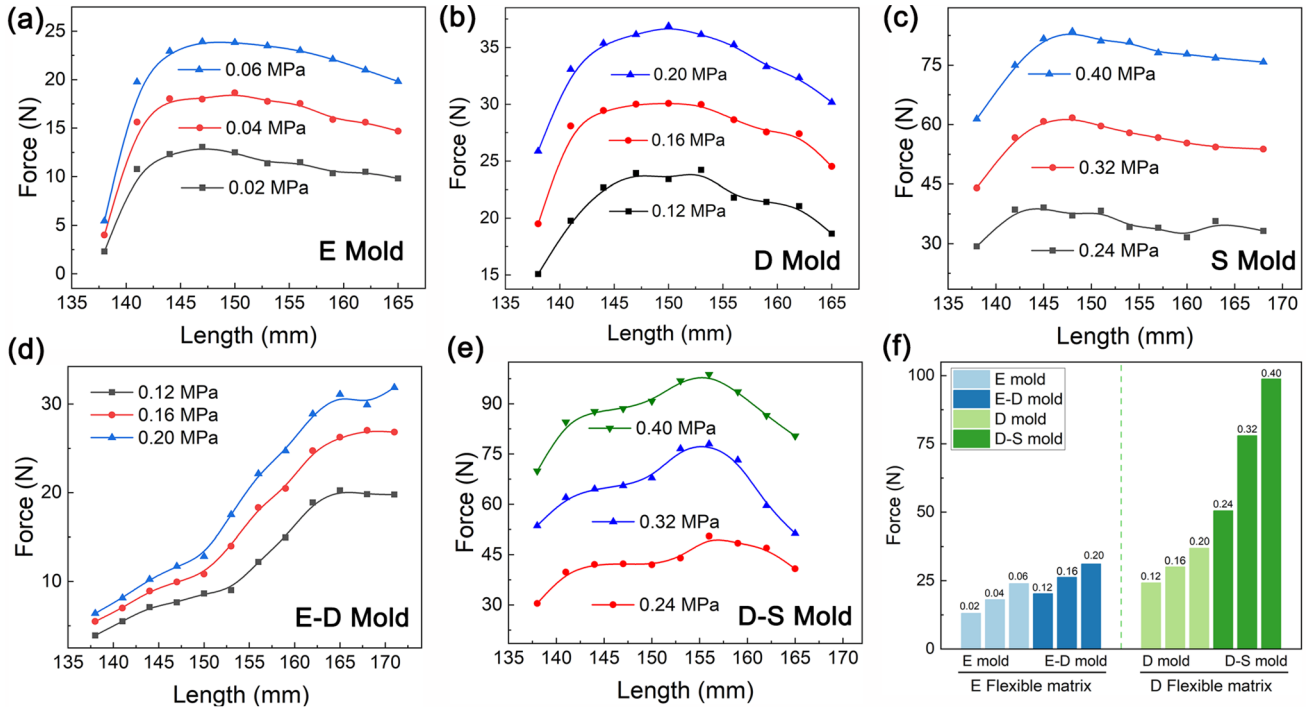


**Fig. 9** Relationship between tetanic force and length of five muscle-like actuators. (**a–e**). Force–length properties of E, D, S, E-D, and D-S molds under different actuation pressures. (**f**) Comparison of force over contractile unit materials of E flexible matrix actuator and D flexible matrix actuator

provides an important design and optimizing strategy for soft actuators.

The force–length and force–velocity properties of an actuator are independent on its building materials. Our results prove that the above design strategy using a structure, architecture, and configuration similar to those of biological muscle is important for optimal mechanical properties. Although the actuator force, velocity, and displacement are largely dependent on their material, contractile units play a primary role in force generation, and the flexible matrix significantly affects subsequent force transmission and deformation, the interaction of contractile units, fluid, and flexible matrix eventually influence the final force, velocity, displacement, and three-dimensional motion of the actuator.

The above findings support the idea that the mechanical output of skeletal muscle is based not only on force generation [30] but also force transmission by the interaction of contractile units and flexible matrix, and their architecture, structure, and morphology [31–33]. In the present study, the D-S mold actuator demonstrated excellent performance in producing high strain and stress due to the capability of the contractile unit for high force generation and that of the flexible material for high force transmission and displacement.

A better understanding of the mechanical behaviors will benefit the improvement of muscle-like actuator performance. Many directions of research are anticipated in the pursuit of improving mechanical performance through exploring new materials, structures, and actuation methods, such as smart materials, hydraulics, and valve control-associated driving. Nonetheless, one outstanding issue remains in that current actuator is cannot directly transmit force because of the flexible actuator ends, which can undergo large deformation after applying external loads, thus allowing the output force to be lost, such as in the case of the E-D mold actuator. There may be an efficient method for improving actuator performance by adding bio-muscle tendons [34, 35] made of flexible and non-stretchable materials, which avoid elastic deformation at two ends, allowing the force to be transmitted from the flexible matrix to external loads. The combination of proposed HimiSK actuators with favorable mechanical properties and bio-tendon development may prove a promising direction toward next-generation muscle-like actuators. To expand the use of muscle-like actuators, the prevailing issues will be addressed in future work.

**Acknowledgements** This work was supported by the National Natural Science Foundation of China (Nos. 52075216, 91948304, and 91848202).

**Author contributions** LR and CBL were involved in conceptualization, YJW was involved in writing—original draft, formal analysis, and visualization; CBL helped in writing—review & editing; LQR contributed to supervision.

## Declarations

**Conflict of interest** The authors declare that there is no conflict of interest.

**Ethical approval** This article does not contain any studies with human or animal subjects performed by any of the authors.

## References


1. Roberts TJ, Eng CM, Sleboda DA et al (2019) The multi-scale, three-dimensional nature of skeletal muscle contraction. Physiology 34(6):402–408. https://doi.org/10.1152/physiol.00023.2019
2. Neptune RR, McGowan CP, Fiandt JM (2009) The influence of muscle physiology and advanced technology on sports performance. Annu Rev Biomed Eng 11:81–107. https://doi.org/10.1146/annurev-bioeng-061008-124941
3. Close RI (1972) Dynamic properties of mammalian skeletal muscles. Physiol Rev 52(1):129–197. https://doi.org/10.1152/physrev.1972.52.1.129
4. Eng CM, Emanuel A, Roberts TJ (2018) Structural determinants of muscle gearing during dynamic contractions. Integr Comp Biol 58(2):208–218. https://doi.org/10.1093/icb/icy054
5. Neptune RR, Kautz SA (2001) Muscle activation and deactivation dynamics: the governing properties in fast cyclical human movement performance? Exerc Sport Sci Rev 29(2):76–80. https://doi.org/10.1249/00003677-200104000-00007
6. Chou CP, Hannaford BN (1996) Measurement and modeling of McKibben pneumatic artificial muscles. IEEE Trans Robot Autom 12(1):90–102. https://doi.org/10.1109/70.481753
7. Hunter IW, Lafontaine S (1992) A comparison of muscle with artificial actuators. Tech Dig IEEE Solid-State Sens Actuator Workshop. https://doi.org/10.1109/solsen.1992.228297
8. Klute GK, Czerniecki JM, Hannaford B (1999) McKibben artificial muscles: pneumatic actuators with biomechanical intelligence. IEEE/ASME Int Conf Adv Intell Mech. https://doi.org/10.1109/aim.1999.803170
9. Saga N, Saikawa T (2008) Development of a pneumatic artificial muscle based on biomechanical characteristics. Adv Robot 22(6–7):761–770. https://doi.org/10.1163/156855308x305317
10. Zhang J, Yin Y (2012) SMA-based bionic integration design of self-sensor–actuator-structure for artificial skeletal muscle. Sens Actuators A Phys 181:94–102. https://doi.org/10.1016/j.sna.2012.05.017
11. Azizi E, Roberts TJ (2013) Variable gearing in a biologically inspired pneumatic actuator array. Bioinspiration Biomim 8(2):026002. https://doi.org/10.1088/1748-3182/8/2/026002
12. Schmitt S, Günther M, Rupp T et al (2013) Theoretical hill-type muscle and stability: numerical model and application. Comput Math Methods Med 2013:1–7. https://doi.org/10.1155/2013/570878
13. Klute GK, Czerniecki JM, Hannaford B (2002) Artificial muscles: Actuators for biorobotic systems. Int J Robot Res 21(4):295–309. https://doi.org/10.1177/027836402320556331
14. Kanik M, Orguc S, Varnavides G et al (2019) Strain-programmable fiber-based artificial muscle. Science 365(6449):145–150. https://doi.org/10.1126/science.aaw2502
15. Kellaris N, Venkata VG, Smith GM et al (2018) Peano-HASEL actuators muscle-mimetic, electrohydraulic transducers that linearly contract on activation. Sci Robot. https://doi.org/10.1126/scirobotics.aar3276
16. Acome E, Mitchell SK, Morrissey TG et al (2018) Hydraulically amplified self-healing electrostatic actuators with muscle-like performance. Science 359(6371):61–65. https://doi.org/10.1126/science.aao6139
17. Shepherd RF, Ilievski F, Choi W et al (2011) Multigait soft robot. PNAS 108(51):20400–20403. https://doi.org/10.1073/pnas.1116564108
18. Wehner M, Truby RL, Fitzgerald DJ et al (2016) An integrated design and fabrication strategy for entirely soft, autonomous robots. Nature 536(7617):451–455. https://doi.org/10.1038/nature19100
19. Yang D, Verma MS, So JH et al (2016) Buckling pneumatic linear actuators inspired by muscle. Adv Mater Technol 1(3):1600055. https://doi.org/10.1002/admt.201600055
20. Diteesawat RS, Helps T, Taghavi M et al (2020) Characteristic analysis and design optimization of bubble artificial muscles. Soft Robot 8:186–199. https://doi.org/10.1089/soro.2019.0157
21. Mintchev S, Floreano D (2016) Adaptive morphology: a design principle for multimodal and multifunctional robots. IEEE Robot Autom Mag 23(3):42–54. https://doi.org/10.1109/mra.2016.2580593
22. Azizi E, Brainerd EL, Roberts TJ (2008) Variable gearing in pennate muscles. PNAS 105(5):1745–1750. https://doi.org/10.1073/pnas.0709212105
23. Holt NC, Danos N, Roberts TJ et al (2016) Stuck in gear: age-related loss of variable gearing in skeletal muscle. J Exp Biol 219(7):998–1003. https://doi.org/10.1242/jeb.133009
24. Gao Y, Zhang C (2015) Structure–function relationship of skeletal muscle provides inspiration for design of new artificial muscle. Smart Mater Struct 24(3):033002. https://doi.org/10.1088/0964-1726/24/3/033002
25. Borg TK, Caulfield JB (1980) Morphology of connective tissue in skeletal muscle. Tissue Cell 12(1):197–207. https://doi.org/10.1016/s0040-8166(81)80005-5
26. Brainerd EL, Azizi E (2005) Muscle fiber angle, segment bulging and architectural gear ratio in segmented musculature. J Exp Biol 208(Pt 17):3249–3261. https://doi.org/10.1242/jeb.01770
27. Roche ET, Wohlfarth R, Overvelde JT et al (2014) A bioinspired soft actuated material. Adv Mater 26(8):1200–1206. https://doi.org/10.1002/adma.201304018
28. Ralston HJ, Polissar MJ, Inman VT et al (1949) Dynamic features of human isolated voluntary muscle in isometric and free contractions. J Appl Physiol 1:526–533. https://doi.org/10.1152/jappl.1949.1.7.526
29. Hill AV (1938) The heat of shortening and the dynamic constants of muscle. Proc R Soc Lond B Biol Sci 126(843):136–195. https://doi.org/10.1098/rspb.1938.0050
30. Millman BM (1998) The filament lattice of striated muscle. Physiol Rev 78(2):359–391. https://doi.org/10.1152/physrev.1998.78.2.359
31. Street SF (1983) Lateral transmission of tension in frog myofibers: a myofibrillar network and transverse cytoskeletal connections are possible transmitters. J Cell Physiol 114(3):346–364. https://doi.org/10.1002/jcp.1041140314
32. Nagel A (1935) Die mechanischen Eigenschaften von Perimysium internum und Sarkolemm bei der quergestreiften Muskelfaser. Cell Tissue Res 22(5):694–706 (in German). https://doi.org/10.1007/bf00380086
33. Nagel A (1934) Die mechanischen Eigenschaften der Kapillarwand und ihre Beziehungen zum Bindegewebslager. Ztschrift Zellforsch Mikrosk Anat 21(3):376–387 (in German). https://doi.org/10.1007/bf00587421
34. Wilson JM, Flanagan EP (2008) The role of elastic energy in activities with high force and power requirements: a brief review. J Strength Cond Res 22(5):1705–1715. https://doi.org/10.1519/jsc.0b013e31817ae4a7
35. Ishikawa M, Komi PV, Grey MJ et al (2005) Muscle-tendon interaction and elastic energy usage in human walking. J Appl Physiol 99(2):603–608. https://doi.org/10.1152/japplphysiol.00189.2005